Continuous Hidden Markov Model for Pedestrian Activity Classification and Gait Analysis

Article *in* IEEE Transactions on Instrumentation and Measurement · May 2013

DOI: 10.1109/TIM.2012.2236792

4 authors:

Ghazaleh Panahandeh
KTH Royal Institute of Technology
24 PUBLICATIONS **156** CITATIONS
SEE PROFILE

Nasser Mohammadiha
Volvo Car Group, Göteborg, Sweden
31 PUBLICATIONS **400** CITATIONS
SEE PROFILE

Arne Leijon
KTH Royal Institute of Technology
86 PUBLICATIONS **1,085** CITATIONS
SEE PROFILE

Peter Händel
KTH Royal Institute of Technology
308 PUBLICATIONS **3,251** CITATIONS
SEE PROFILE

Continuous Hidden Markov Model for Pedestrian Activity Classification and Gait Analysis

Ghazaleh Panahandeh, *Student Member, IEEE*, Nasser Mohammadiha, *Student Member, IEEE*, Arne Leijon, *Member, IEEE*, and Peter Händel, *Senior Member, IEEE*

***Abstract*—This paper presents a method for pedestrian activity classification and gait analysis based on the microelectromechanical-systems inertial measurement unit (IMU). The work targets two groups of applications, including the following: 1) human activity classification and 2) joint human activity and gait-phase classification. In the latter case, the gait phase is defined as a substate of a specific gait cycle, i.e., the states of the body between the stance and swing phases. We model the pedestrian motion with a continuous hidden Markov model (HMM) in which the output density functions are assumed to be Gaussian mixture models. For the joint activity and gait-phase classification, motivated by the cyclical nature of the IMU measurements, each individual activity is modeled by a "circular HMM." For both the proposed classification methods, proper feature vectors are extracted from the IMU measurements. In this paper, we report the results of conducted experiments where the IMU was mounted on the humans' chests. This permits the potential application of the current study in camera-aided inertial navigation for positioning and personal assistance for future research works. Five classes of activity, including walking, running, going upstairs, going downstairs, and standing, are considered in the experiments. The performance of the proposed methods is illustrated in various ways, and as an objective measure, the confusion matrix is computed and reported. The achieved relative figure of merits using the collected data validates the reliability of the proposed methods for the desired applications.**

***Index Terms*—Activity classification, gait analysis, hidden Markov model (HMM), inertial measurement unit (IMU).**

I. Introduction

RECENTLY, considerable research within the instrumentation and measurement community has been devoted to the application of microelectromechanical systems (MEMS) inertial sensors in different areas such as inertial navigation [1]–[3], vehicle applications [4], [5], behavioral analysis [6], and biomedical applications [7], [8]. This is mainly motivated by the development of the MEMS technology to provide such a lightweight and cheap motion capture sensor, which is becoming a standard feature of smartphones and personal digital assistants. Hence, MEMS inertial measurement units (IMUs) can be considered as fundamental and primary motion capture sensors. IMU sensors have been successfully used in human locomotion analysis such as human activity monitoring, gesture recognition, fall detection, balance control evaluation, and abnormal behavior detection [9]–[13]. Another widely investigated application of IMU is in inertial navigation systems, which has recently received increasing attention in the instrumentation and measurement community, e.g., personal navigation and dead reckoning [14]–[16], and road vehicle navigation [17].

IMU-based positioning systems, however, suffer from integration drift; small errors in the measurement of acceleration and angular velocity are integrated into progressively larger errors in velocity, which are compounded into still greater errors in position. Therefore, the estimated pose must be periodically corrected by additional information. This information can either be provided by an additional sensor, such as a GPS [18]–[20] and a camera [1], [21], or an algorithm that intelligently takes into account the state of the system, e.g., zero velocity update (ZUPT) in foot-mounted IMU pedestrian navigation [14], [22], [23]. However, in the commonly used threshold-based ZUPT methods, integrating activity classification and dead reckoning techniques can lead to a better choice for the threshold value and therefore can improve the performance of the navigation system [24], [25]. Apart from the foot-mounted IMU, pedestrian vision-aided inertial navigation systems can be counted among the most reliable positioning systems if the activity type of the moving subjects can be integrated with the image data (to avoid motion blurred images and provide step information) [1], [26].

Human activity classification is also an important aspect of disease diagnosis and assistance health care in medical centers, with, for instance, early fall detection to rescue subjects [27], [28] and metabolic energy expenditure [13], [29]. In addition to the activity classification, reliable gait-phase classification is an important topic for human locomotion analysis and identifying abnormality [7], [8], [30]. Moreover, the referred step information in the two mentioned positioning systems is closely related to the gait analysis. Gait analysis involves the recognition of the underlying gait phases; a gait phase is defined as a state of the body during the stance and swing phases of each step while walking, running, etc. Among the gait-phase classification methods, we can refer to threshold-based approaches [30], [31] and fuzzy logic methods [8] in which the system must be individually calibrated for different users.

The current activity and gait-phase classification methods, however, suffer from a lack of robustness, e.g., they are threshold based [30], [31], have to be calibrated for different individuals [8], or are not suitable for vision-aided inertial navigation

Manuscript received June 21, 2012; revised September 9, 2012; accepted November 20, 2012. Date of publication January 17, 2013; date of current version April 3, 2013. Parts of this work have been supported by The Swedish Agency for Innovation Systems (VINNOVA). The Associate Editor coordinating the review process for this paper was Dr. Kurt Barbe.

The authors are with the School of Electrical Engineering, ACCESS Linnaeus Centre, KTH Royal Institute of Technology, SE-10044 Stockholm, Sweden (e-mail: ghpa@kth.se; nmoh@kth.se; leijon@kth.se; ph@kth.se).

Color versions of one or more of the figures in this paper are available online at http://ieeexplore.ieee.org.

Digital Object Identifier 10.1109/TIM.2012.2236792

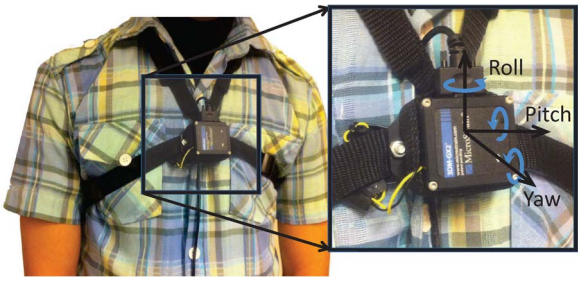

Fig. 1. Illustration of Chem-IMU. The black box indicates the IMU sensor mounted on the chest of a sample participant. The drawing axes on the IMU illustrate approximately the direction of the accelerometers and gyroscopes' measurements.

systems because they are developed for foot-mounted IMU [24]. Moreover, the joint activity and gait-phase classification has not been fully considered in the available literature.

The main contribution of the current study is to develop a probabilistic user-independent approach for activity and gait-phase classification using an upper body positioned IMU, specifically, chest-mounted IMU (Chem-IMU); see Fig. 1. The upper body positioned IMU experiences less vibration and noise during movement compared to the lower body positioned IMU [32]; additionally, it provides a wide field of view for a camera to be used in the vision-aided inertial navigation systems [1], [21], [26], [33], [34].

The proposed novel classification methods are based on the hidden Markov model (HMM). In this application, the hidden states are, in fact, different activity classes or gait phases. Since the IMU measurements are usually quantized with a large number of bits, we propose using a continuous HMM (HMM with continuous output density functions) rather than a discrete HMM as in [10], [35], and [36]. The state-conditional output density functions of HMM are assumed to be a Gaussian mixture model (GMM) that is powerful in modeling any continuous distribution desired. We propose two HMM-based solutions for the following: 1) activity classification and 2) joint activity and gait-phase classification. The proposed activity classification is based on the method introduced in [37]. The joint activity and gait-phase classification is achieved via the modeling of IMU measurements within each activity type using a circular HMM. Given that no other algorithm is proposed in the literature for the considered Chem-IMU setup (to the best of our knowledge), the performance of the proposed classification techniques is self-analyzed, and the correct classification rate is calculated as the relative figure of merit. The achieved promising results verify the merit of the proposed algorithms for the desired applications.

This paper is organized as follows: The measurement and sensor model is described in Section II, the problem description and the proposed classification methods are presented in Section III, experimental validation is reported in Section IV, discussion is given in Section V, and finally, the conclusion of the study is summarized in Section VI.

II. Measurement and Sensor Model

The classification of pedestrian activity is achieved by using the measurements from the three orthogonal gyroscopes and

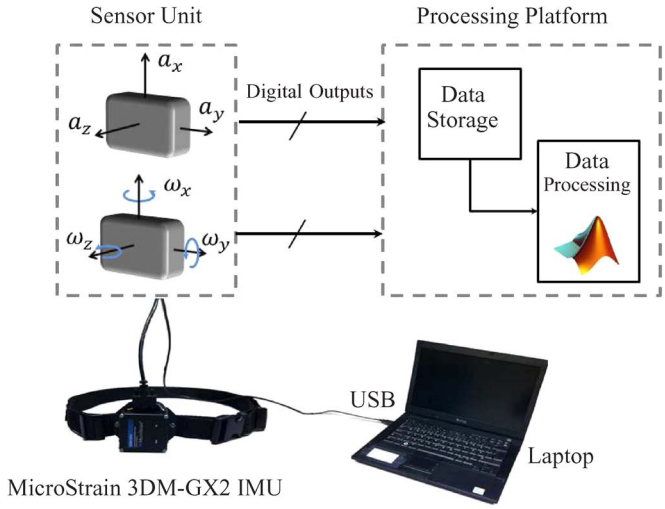

Fig. 2. Overall system architecture. The sensor module, considered to be an IMU, consists of three orthogonal accelerometers and three orthogonal gyroscopes. The stored IMU measurements are processed by a laptop to perform the classification. This occurs in the processing platform.

the three orthogonal accelerometer clusters of the IMU. A MicroStrain 3DM-GX2 IMU was used in the experiments. This converts the motion sensors' raw voltage outputs into a digital format (in terms of A/D converter codes) with a sampling rate of 250 Hz. The accelerometer measurements are then rescaled into physical units of grams ($1\ \mathrm{g} = 9.80665\ \mathrm{m/s^2}$). Independent of the IMU's position, the measurements of the accelerometer, $\mathbf{a}_k \in \mathbb{R}^3$, and the gyroscope, $\boldsymbol{\omega}_k \in \mathbb{R}^3$, clusters of the IMU, as shown in Fig. 2, are modeled as

$$\mathbf{y}_k = \mathbf{x}_k + \mathbf{n}_k \in \mathbb{R}^6 \tag{1}$$

where

$$\mathbf{x}_k = \begin{bmatrix} \mathbf{a}_k \\ \boldsymbol{\omega}_k \end{bmatrix} \qquad \text{and} \qquad \mathbf{n}_k = \begin{bmatrix} \mathbf{n}_k^{\mathbf{a}} \\ \mathbf{n}_k^{\boldsymbol{\omega}} \end{bmatrix}.$$

$\mathbf{n}_k^{\mathbf{a}} \in \mathbb{R}^3$ and $\mathbf{n}_k^{\boldsymbol{\omega}} \in \mathbb{R}^3$ are noise vectors associated with the acceleration and angular rates, respectively. k is the corresponding sample index.

For the data collection, users were asked to connect the IMU to their chest, with no particular consideration to the IMU placement, as illustrated in Fig. 1. It should be noted that mounting the sensor in slightly different positions, on different individuals, or in different environments may cause additional noise or biases in the measurements. Moreover, due to the random nature of the additive noise, (1) should rather be analyzed stochastically. In the proposed methodology (see Section III), these issues are recalled and are solved by applying a proper preprocessing and modeling of the signal.

Fig. 2 provides a general overview of the system architecture. The IMU sensor unit is shown on the left-hand side. The sensor module carried by the participants is directly connected to a laptop via a USB port. The IMU measurements are first stored in the processing platform, and then, the classification is done offline at MATLAB via the processing module.

Although the primary goals of this work are pedestrian activity and gait-phase classification through a wearable IMU, we are also interested in the future application of the classifier

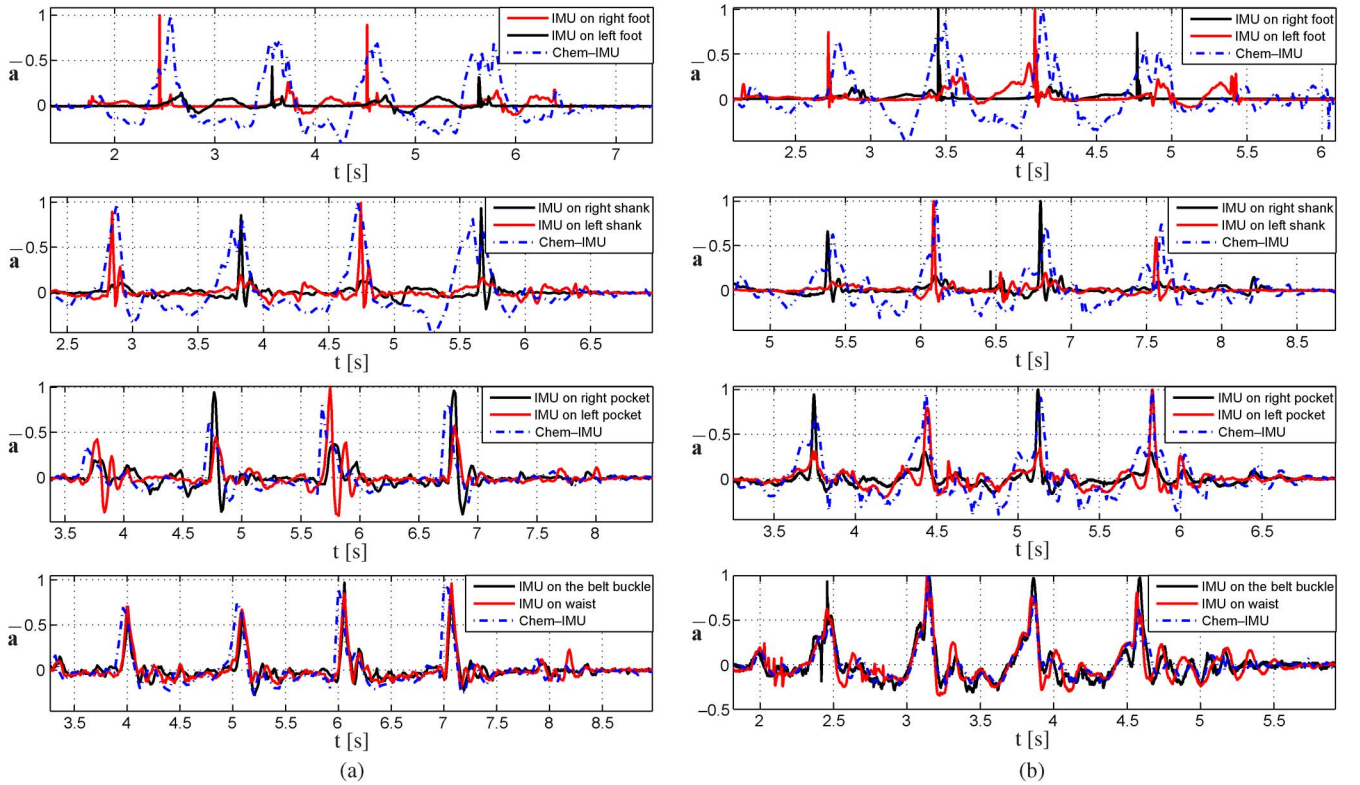

Fig. 3. Comparison between the cyclical pattern of the Chem-IMU and the IMUs mounted on the following: feet, shanks, pockets, waist (close to L3 vertebra), and belt buckle. The vertical axes indicate the normalized norm of the accelerometers' measurements $\bar{\mathbf{a}} = \|\mathbf{a}\| / \max(\|\mathbf{a}\|)$. (a) First subject with height of 185 cm. (b) Second subject with height of 167 cm.

where the IMU is coupled with a secondary vision system for inertial navigation. As a result, the IMU is considered to be placed on the chest. However, the proposed methods are not restricted to the Chem-IMU setup, and they can be used for different IMU placements on the human body as far as the IMU signals present a cyclical nature corresponding to the human motions. Fig. 3 represents such cyclical patterns for different IMU body placements for two sample participants. In this figure, the vertical axes indicate the normalized norm of the accelerometer measurements. Four different experiments were done in which the Chem-IMU signals were compared with the measurements from IMUs placed on different parts of the subject's body as follows: feet, shanks, pockets, on the waist close to the L3 vertebra, and, finally, on the belt buckle. In the normal walking scenario, each step is due to the movement of one of the legs while the other leg's foot is stationary on the ground. Hence, to totally represent four steps, two IMUs were placed symmetrically on both the right and left legs; meanwhile, a single upper body positioned IMU can provide the full representation of each step.

III. Activity and Gait-Phase Classification

A. Problem Description

Walking is characterized by the cyclical movements of the lower limbs [9], in which the stance and swing phases define each gait cycle. However, using the measurements from the IMU mounted on the other parts of the body (see Fig. 3), a similar analysis can be performed to define different gait cycles. In the proposed methods, the following classes of activity are considered for classification: walking, running, going upstairs, going downstairs, and standing (no rigid body acceleration). This latter state corresponds to the case when the user is standing still; however, no restriction for the rotation is considered. Represented symbolically

$$\frac{1}{L}\sum_{k=1}^{L}\|\mathbf{a}_k\| \approx g \tag{2}$$

where L is the length of the analysis window, g is the magnitude of the local gravity vector, and $\|\cdot\|$ indicates the norm operation. Although only five categories of the human physical activities are considered in this study, other activities such as bending, sitting down, and standing up can also be considered as additional states in the proposed classification approaches.

B. Methodology

Both of the proposed methods for the activity and the joint activity and gait-phase classification consist of three steps: 1) preprocessing; 2) feature extraction; and 3) classification.

The digital preprocessing module of the system is a bandpass filter that reduces measurement noise and removes the effect of the IMU displacement on the chest for different subjects. The bandpass filter is a combination of a standard low-pass filter $f_{\text{cutoff}} = 20$ Hz) and a dc level cancelation.

To both gain a better description of the signals' characteristics and reduce the dimensions of the signal, a feature extraction method is used once the noise reduction has been applied to the IMU measurements. The extracted feature vectors should best discriminate between different patterns. Various kinds of

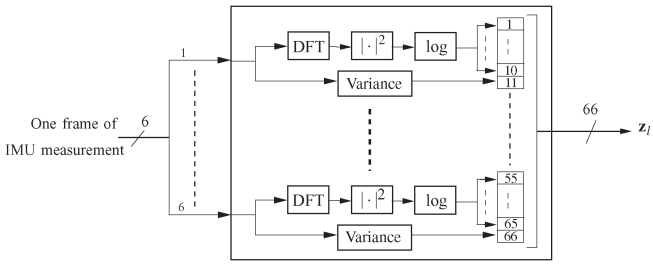

Fig. 4. Illustration of the feature vector $\mathbf{z}_l$ used for activity classification. For each segment of data, the logarithm of the first ten magnitude-squared DFT coefficients and the variance of the data are used to construct $\mathbf{z}_l$.

feature extraction methods have been considered for activity classification in the literature such as vector quantization [10], principal component analysis [38], frequency analysis [36], and time–frequency analysis [39]. A comprehensive study on the sensor-based feature extraction methods for activity classification can be found in [9], [40], and [41]. Depending on the considered problem, two different types of feature extraction methods are used in this paper. The details of the feature extraction units and the classification techniques are given in the following.

1) Activity Classification: In this problem, we focus on the pedestrian activity classification in which further analysis of the underlying gait cycle (a period of the IMU measurement during each activity) is not of interest. To exploit the prior knowledge that the type of activity does not change rapidly, it is proper to use the long-term properties of the IMU signals to recognize the activity type. Therefore, time–frequency domain analysis is used for the feature extraction. For human activity, the IMU measurements are assumed to be a locally stationary stochastic process within short windows up to 1–2 s; that is, 250–500 samples at a 250-Hz sampling rate. Hence, we apply a discrete Fourier transform (DFT) to the signals with overlapped short time frames. The frame length should be chosen such that the signal can be considered stationary within each frame while the overlap length influences the update frequency of the classification results. In our experiments, the frame length was chosen to be 512 samples with 75% overlap between consecutive frames. The windowing of the signal into the short time frames was done using a Hann window rather than a rectangular window to reduce the edge effects of the windowing. Furthermore, the DFT length was chosen to be equal to the length of the short time frames, which corresponds to a 512-point DFT in our setup. For the feature extraction, the first ten DFT coefficients (coefficients 1 to 10) of the IMU measurements are transferred to the log-spectral domain by taking the logarithm of the magnitude-squared DFT coefficients. Then, the obtained features for each of the IMU signals are concatenated to make a 60-length vector for the current time frame. The variances of the signals in each segment are also explicitly concatenated to these vectors to obtain the complete feature vector that is represented by $\mathbf{z}_l$ in the following (see Fig. 4).

The described TF analysis implies that the classification result always has a lag that is approximately equal to the "frame length-overlap length." However, this delay is tolerable in pedestrian activity classification. In our setup, it corresponds to 128 samples. The nice property of the TF analysis is that

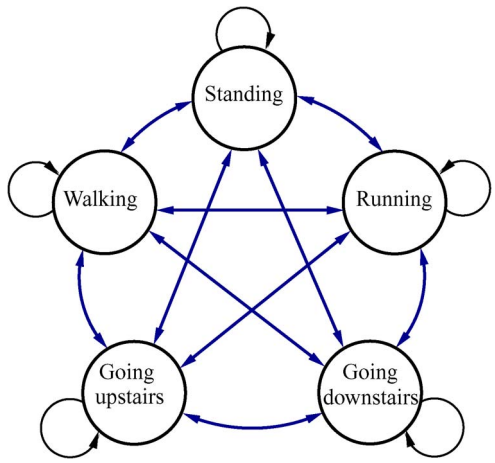

Fig. 5. Architecture of the considered HMM for activity classification.

different activities are easily discriminated based on their frequency characteristics. For instance, the usual cycle duration of walking is around 0.5–1 s, meaning that the sinusoidal harmonic at 1–2 Hz in the frequency analysis will have the highest energy. On the other hand, with running for example, the sinusoidal harmonic at 4–6 Hz will have the highest energy.

Here, the human activity is modeled with a continuous HMM using a first-order Markov chain; thus, an HMM which has five states corresponding to five different activity classes is applied to classify the obtained feature vectors (see Fig. 5). The components of the HMM classifiers are schematically illustrated in Fig. 6. In this figure, an internal source category (standing, walking, etc.) generates a signal ,and the goal is to recognize the signal source in the classifier. Noise can be added to the system at several points. Feature vector $\mathbf{Z}_l$ is obtained in the feature extraction part and is passed to the classifier. The HMM classifier consists of two objects: a discrete first-order Markov chain and the probability density functions of the feature vectors that are considered to be GMMs in this paper. To deal with the previously mentioned measurement noise and IMU displacement variation, feature vectors are modeled with continuous GMMs as

$$f_{\mathbf{Z}_l|S_l}(\mathbf{z}_l|S_l=i)=\sum_{m=1}^{M} w_{m,i}\mathcal{N}(\mathbf{z}_l;\mu_{m,i},C_{m,i}) \qquad (3)$$

where $\mathcal{N}(\mathbf{z}_l;\mu_{m,i},C_{m,i})$ represents a multivariate Gaussian distribution with mean vector $\mu_{m,i}$ and covariance matrix $C_{m,i}$. Moreover, $\sum_{m=1}^{M} w_{m,i}=1$. In the experiments, we set empirically $M=3$, and the covariance matrices were restricted to be diagonal. While the correlations between different features are captured by using the mixture distribution, the assumption of diagonal covariance matrices reduces the number of the unknown parameters that must be estimated, which is beneficial in dealing with low amount of training data. As a result, the considered HMM is characterized by the parameters of the Markov chain $\{A,q\}$ and the parameters of the state-conditional output probability density functions, i.e., parameters of the GMMs $\{\mu,C,w\}$. The transition matrix of the Markov chain, A, models the slow changes in the type of the activity, and its elements are defined as $a_{i,j}=p(S_{l+1}=j|S_l=i)$, where S_l

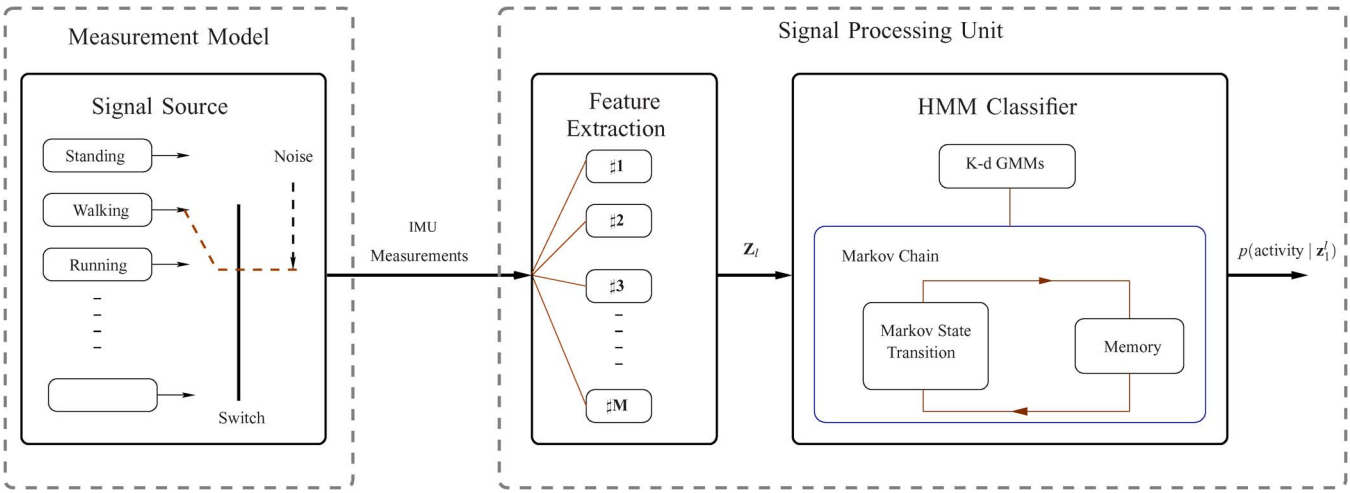

Fig. 6. Schematic representation of the developed system. The signal source block models the pedestrian activity behavior using a switch structure. In the proposed solution, a proper feature vector is first extracted from the IMU measurements, and then, an HMM-based classifier is applied to find the posterior probability of each of the possible activity classes.

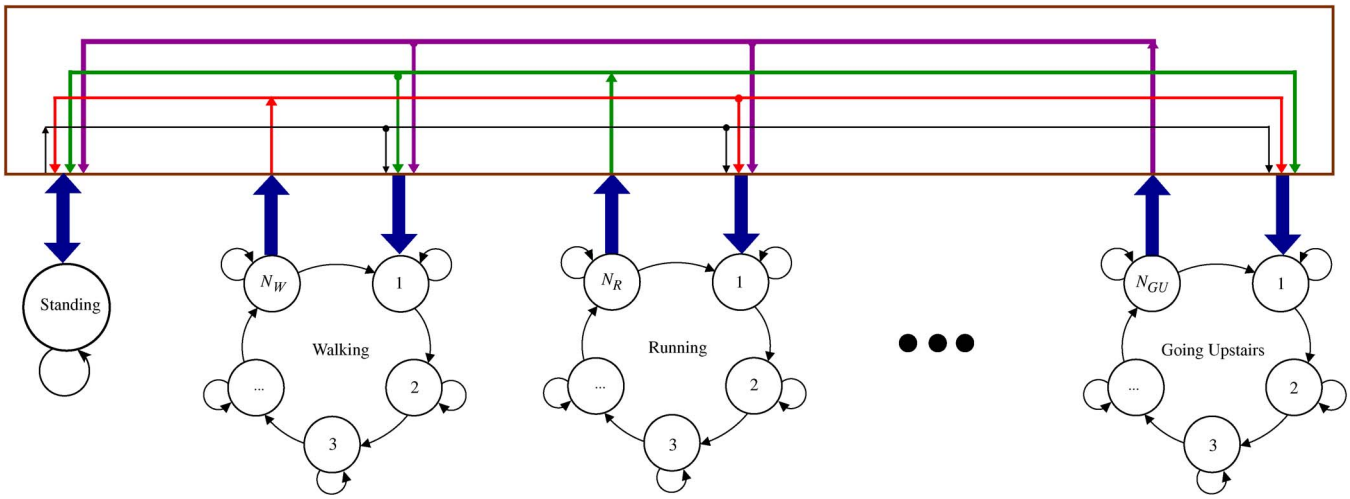

Fig. 7. Architecture of the circular HMM with the corresponding sub-HMMs for different activities. All the sub-HMMs are connected together to design a single HMM that models pedestrian activity.

denotes the activity type in time frame l and is referred to as the hidden state. The vector q is the initial state probability mass function with $q_j = p(S_1 = j)$. In the current model, it makes sense to predefine A and q based on some sensible values of the tendency of humans to switch between different activity types; therefore, we set

$$q \in \mathbb{R}_{\geq 0}^{5\times 1}, \quad q_j = \begin{cases} 1 & \text{for } j = 5 \text{ (Standing)} \\ 0 & \text{for } j \neq 5 \end{cases}$$

$$A \in \mathbb{R}_{\geq 0}^{5\times 5}, \quad a_{i,j} = \begin{cases} 0.9 & \text{for } i = j \\ 0.025 & \text{for } i \neq j. \end{cases}$$

The estimation of the GMM parameters is done using an expectation maximization (EM) algorithm [42], [43]. In the test phase, the classification is done by applying the forward algorithm [44] to find the probability for each of the aforementioned states given all the current and previous measurements from the IMU, i.e., $p_{S_l|\mathbf{z}_1^l}(S_l = i|\mathbf{z}_1^l)$, where $\mathbf{z}_1^l$ denotes the feature vectors measured from time frame 1 until l, i.e., $\mathbf{z}_1^l = \{\mathbf{z}_1, \ldots \mathbf{z}_l\}$. The most probable state can be considered as the output of the classification procedure.

2) Joint Activity Classification and Gait Analysis: For this problem, a classification algorithm is developed that simultaneously classifies the pedestrian activity and the gait phase of each gait cycle, i.e., a substate of the pedestrian activity. Similar to Section III-B1, the pedestrian activity is modeled with a continuous HMM. However, each gait cycle of the IMU signals which corresponds to one step is further modeled with a smaller circular HMM. In this case, each state of these circular HMMs corresponds to one gait phase. This is motivated by the fact that the IMU signals reveal cyclical patterns for most of the pedestrian activities. In other words, different HMMs, conditioned on a specific activity type, are forced to have a circular structure whenever it is appropriate. In the following, these circular HMMs are referred to as sub-HMMs. The higher layer HMM, which models the human activity, is obtained by combining all of the circular HMMs. The explained circular HMMs are left-to-right HMMs (where only transitions from one state to the next state are allowed) with an additional property that the last state is connected to the first state; Fig. 7 demonstrates the structure of the designed sub-HMMs and their integrations to create the higher layer HMM. In this case, a

different number of states should be considered for the sub-HMMs depending on the activity type. In our experiments, we trained four states for all the activity classes except standing which was modeled by a single state.

In a similar vein to Section III-B1, instead of the raw IMU measurements, feature vectors are obtained and are fed into the HMMs. For this purpose, the IMU signals are segmented and windowed into overlapped short time frames. The signal windowing was done using a frame length of 20 samples with 75% overlap. In this paper, four features are computed for each given short time frame. These include the following: 1) mean; 2) variance; 3) slope; and 4) curvature. A second-order polynomial was fitted to the data in each segment, and the slope and curvature were calculated by taking the first and second derivatives of the signal, respectively. The final feature vector is then constructed by concatenating all the feature vectors for each of the IMU output signals. As before, the distribution of the feature vectors is assumed to be GMM. For the implementation, two Gaussian components were considered for each state of the sub-HMMs, and both were restricted to have diagonal covariance matrices.

Each circular sub-HMM is identified by its Markov chain parameters $\{A, q\}$ and GMM parameters $\{\mu, C, w\}$, as given in (3). The transition matrix for an N-state circular sub-HMM will look like this

$$A = \begin{bmatrix} a_{11} & a_{12} & 0 & \dots & 0 \\ 0 & a_{22} & a_{23} & \dots & 0 \\ \vdots & \vdots & \ddots & \ddots & \vdots \\ 0 & 0 & \dots & a_{N-1,N-1} & a_{N-1,N} \\ a_{N,1} & 0 & \dots & 0 & a_{N,N} \end{bmatrix}.$$

Given the training data for different pedestrian activities, the parameters of different sub-HMMs are estimated using the Baum–Welch algorithm [42], [44], which is an EM algorithm, to obtain maximum likelihood estimates of the desired parameters. Then, to obtain the general HMM for describing the pedestrian activity, all the sub-HMMs are combined together. Hence, the number of the states for this HMM is equal to the sum of the number of the states for all the sub-HMMs. For this HMM, all the elements of the initial state probability vector corresponding to the first state of the sub-HMMs are set to have the same value (equiprobable states). Also, the state-conditional output distribution functions are taken from the sub-HMMs. After putting the transition matrices of the sub-HMMs at the proper positions in the transition matrix, some small heuristic transition probabilities are set to allow transitions from the last state of each sub-HMM to the first state of all the other sub-HMMs. Finally, all the rows are normalized to create a valid transition probability matrix.

After the training, the classification is done by applying the forward algorithm [44], similarly to Section III-B1, to find the probability for each of the aforementioned substates given all the current and previous measurements from the IMU, i.e., $p_{S_l|\mathbf{z}_1^l}(S_l = i|\mathbf{z}_1^l)$, where S_l denotes the hidden state in short time frame l, i.e., S_l corresponds to a specific gait phase from a particular activity type. As a result, the most probable state can be used to infer the gait phase and the activity type simultaneously.

In general, any state from a circular HMM can be considered as the initial state; therefore, a circular HMM does not require any reference point in the input signals for training and testing. However, if the defined initial and final states are supposed to correspond to specific gait phases, it is important to initialize the GMM components in a clever way, e.g., by segmenting each cycle of the IMU output signals into equal parts, then, the first segments of each of the signals' cycles are used to initialize the parameters of the first state. In the current application, it makes sense to consider the first and last states as the beginning and the end of one step. Then, different phases of human gait can be inferred by looking at the corresponding state. Fig. 8(d) shows an example; this figure shows the first IMU output signal (a_x) together with the classified states for walking and running. As it is shown, state indices 4 and 8 correspond to the zero-crossing phases of their corresponding activity types, walking and running, respectively.

IV. Experiments

The main contribution of this work is the proposed probabilistic user-independent classification methods for the specifically defined setup, i.e., Chem-IMU, which facilitate the application of this setup in different areas such as vision-aided inertial navigation. The performance of the proposed algorithms is analyzed both qualitatively and quantitatively in this section.

A. Subject Selection

In order to obtain a sufficient amount of data for training, ten subjects—three females and seven males—participated in the experiment; Table I summarizes both the train-set and test-set subjects' personal characteristics. All the participants were healthy researchers, without any abnormality in their gait cycles, at the Signal Processing Lab and Communication Theory Lab at KTH. None of the train-set subjects were included in the test set during the evaluation process. Similar patterns were observed in the IMU measurements independently of its position on the chest (affecting the dc level of the signals). Table II provides the approximate cumulative length of the test signals for all the considered classes. Moreover, the approximate lengths of the recorded activities for the training phase are as follows: walking $= 25$ min, running $= 3$ min, going upstairs $= 2.5$ min, going downstairs $= 2.5$ min, and standing $= 3$ min.

B. Performance Evaluation

For presentation purposes, the dc levels of the IMU signals are removed in the following figures. Table III shows the corresponding state indices for different activities in both the first and second proposed methods. The performance of the proposed classification approaches is demonstrated in Fig. 8 for different combinations of the activities. The figure presents the first IMU output signal, which corresponds to the orthogonal acceleration, a_x. The results of the classification methods are also plotted over the same signal with red color. The top panel shows the results of the first proposed method, and the bottom

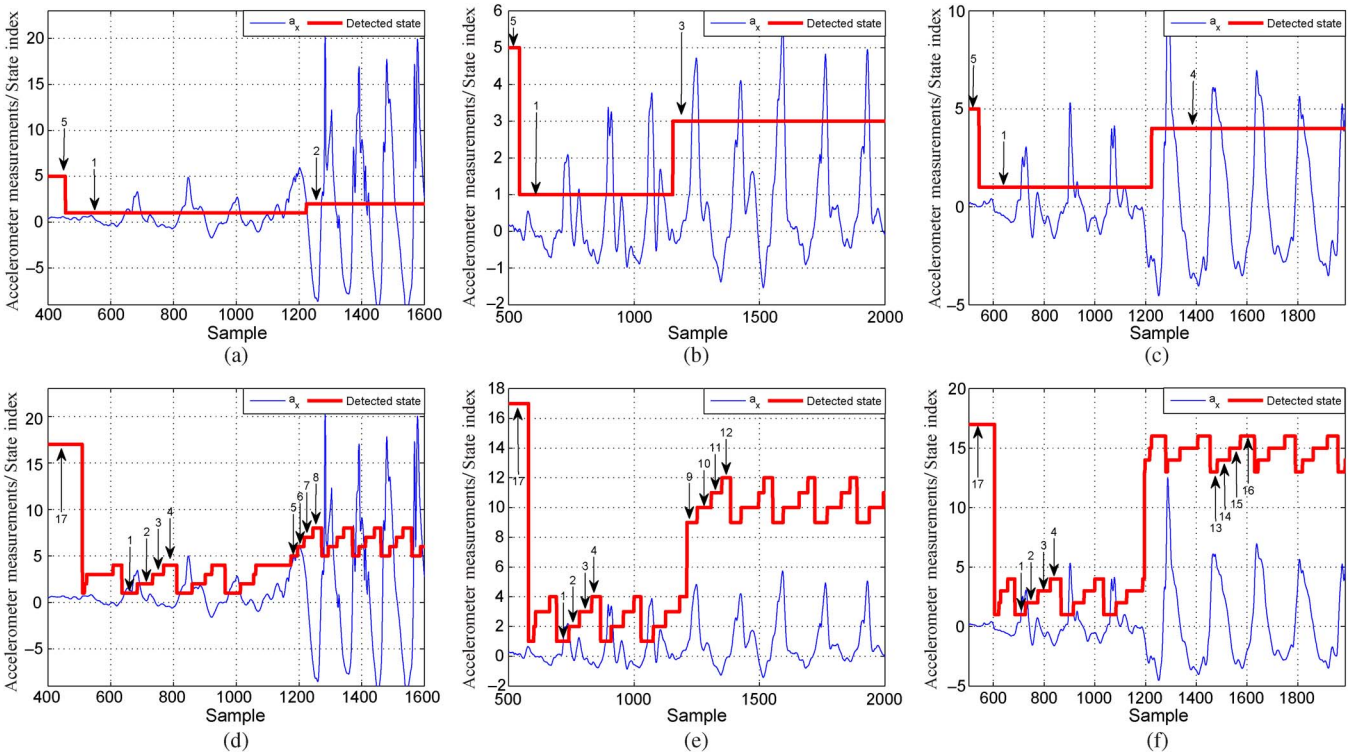

Fig. 8. First IMU output signal (a_x), for the defined activity classes along with the classified activities in subfigures (a), (b), and (c), and the classified joint activity and gait phases in subfigures (d), (e), and (f). The classified activity and gait phases are labeled by their corresponding state indices as described in Table III.

TABLE I
TRAIN-SET AND TEST-SET SUBJECTS' PERSONAL CHARACTERISTICS

	Number of subjects	Height	Weight	Age
Train	10	174±12	68.7±12.5	29.5±4
Test	4	175±11	74.5±12	30±4.9

panel shows the results of the joint activity and gait-phase classification, the second proposed method. Fig. 8(a) and (d) illustrate the orthogonal acceleration signal of the IMU when the user moves from standing to walking and finishes running. Respectively, Fig. 8(b) and (e) represent the sequence of standing → walking → going downstairs. Finally, Fig. 8(c) and (f) show the sequence of standing → walking → going upstairs. Comparing the states' numbers in these figures with Table III verifies that both of the proposed methods have recognized the underlying activity type correctly. It is also interesting to notice how the duration of the gait-phase states [bottom panel of Fig. 8(d)–(f)] varies in different scenarios within each activity class. A simple example of this behavior can be seen in Fig. 8(d); during the transition from walking to running, between samples 1000 and 1200, when the underlying signal does not fit either the walking or running states properly, the state index 4 (last state of the walking) is prolonged unusually until the signal can be explained reasonably well by the running model, and then, the activity is classified as running by transiting from state index 4 to state index 5 (the first state of running).

The evaluations show that most wrong classifications happen during transitions between activities. To demonstrate this phenomenon, the IMU measurements were continuously recorded for a set of activities. Fig. 9 presents the six IMU measurements; three acceleration $[a_x, a_y, a_z]$ signals are plotted in the top panel while three angular rotations $[\omega_x, \omega_y, \omega_z]$ are plotted in the bottom panel. For the sake of visibility, the normalized IMU measurements are shifted along the y-axes. The signals present the following activities: standing → walking → standing → running → standing → going downstairs → standing → going upstairs → standing. During the standing periods, the subject was asked to turn around without changing his position; this type of turning around is mostly visible in the gyroscope measurements and is included in the standing state as mentioned before.

For this example, the classified activities and gait phases are plotted over the first IMU output signal, a_x, in Figs. 10 and 11, respectively. For clarity, some important segments of Fig. 11 are zoomed and plotted in the bottom panel of the same figure. As can be seen in the figures, almost the same types of misclassification happen using both of the developed methods during the transitions. Incorrect classifications during transitions mainly occur because of the body configuration switching from one activity type to another. Therefore, the IMU measurements cannot be modeled with either the preceding or the following activity type well enough. As a result, the system mistakenly recognizes the underlying activity type.

To evaluate the correct activity classification rate of the proposed methods, a supervised classification was performed for which all the data were labeled manually. For this purpose, all the test-set subjects (see Table I) were asked to perform natural activities, including standing, walking, running, going downstairs, and going upstairs, in an indoor environment and with frequent transitions between the activities.

TABLE II
APPROXIMATE CUMULATIVE LENGTH OF THE TEST SIGNALS

		Walking	Running	Going upstairs	Going downstairs	Standing
	Recorded data (min)	12	3.4	2.5	2.5	3
Number of decision	Activity classification	1440	408	300	300	360
	Joint activity and gait-phase classification	1440	816	300	300	720

TABLE III
CONSIDERED CLASSES OF THE ACTIVITIES AND CORRESPONDING STATE INDICES IN THE TRAINED MODELS

	Walking	Running	Going upstairs	Going downstairs	Standing
Activity classification	1	2	3	4	5
Joint activity and gait-phase classification	1→4	5→8	9→12	13→16	17

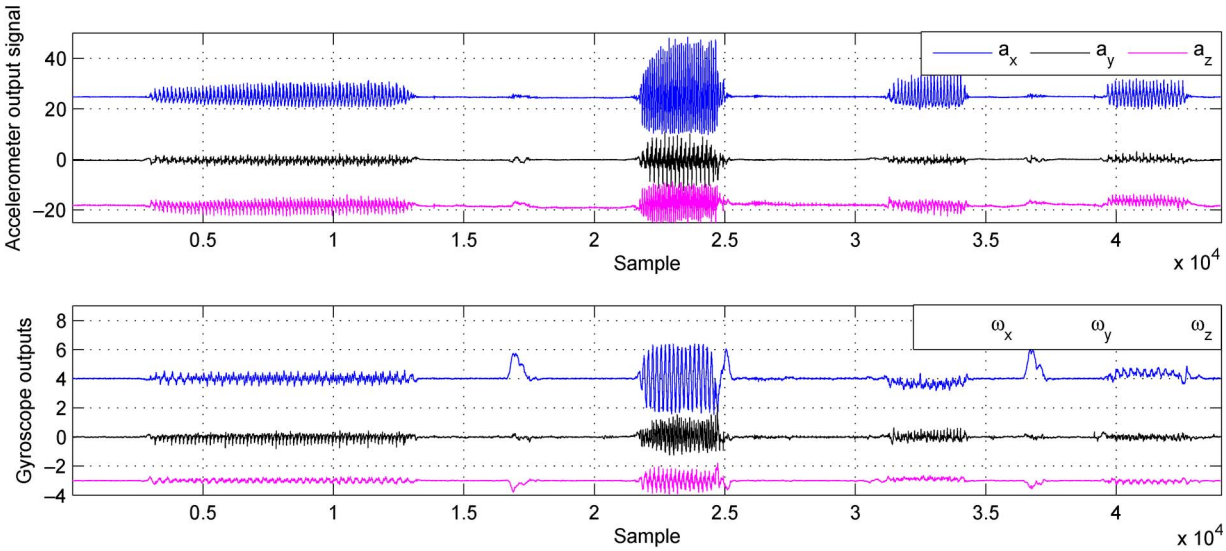

Fig. 9. IMU measurements, accelerometers, and gyroscopes, for all the five defined states. For the sake of visibility, signals are shifted over the y-axes. The signals correspond to the following activities: standing → walking → standing → running → standing → going upstairs → standing → going downstairs → standing.

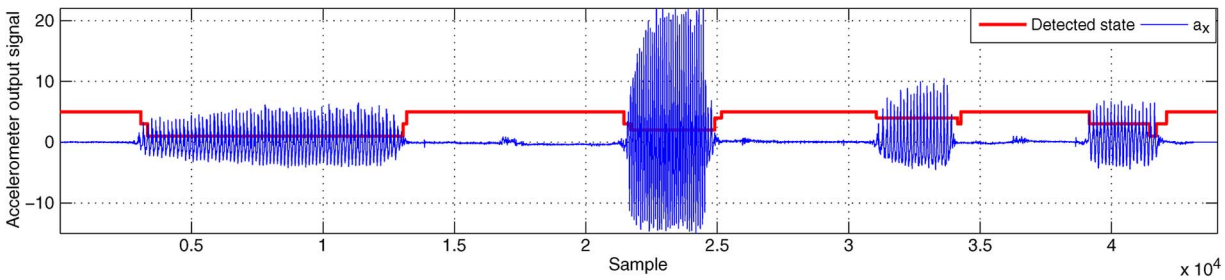

Fig. 10. First IMU output signal (a_x) for all the five defined motion states together with the classified activities based on the first method; see Section III-B1 (see Table III for the state indices). The corresponding IMU measurements are plotted in Fig. 9.

The correct activity classification rate averaged over all the test-set subjects is reported in Tables IV and V for the first proposed method and the second proposed method, respectively. The results are reported in the form of a confusion matrix. Each column of this matrix represents the instances from the classified classes, while each row represents the instances from the actual classes. Hence, the diagonal cells of the tables report the correct classification rate for the corresponding activity. The achieved results for both of the proposed algorithms indicate a promising performance; a rate of about 95% correct classification (with marginally better performance for the second method). Even though this rate is good enough for the desired applications, it should be highlighted that, under the stationary conditions (when the subject does not change his/her activity type rapidly), the correct classification rate would be even higher. This is because most incorrect classifications took place during the switching time between activities, and in our test set, subjects were asked to switch between different activities more frequently than in a daily-life scenario. Thus, the reported classification rate is a pessimistic bound on the achievable result.

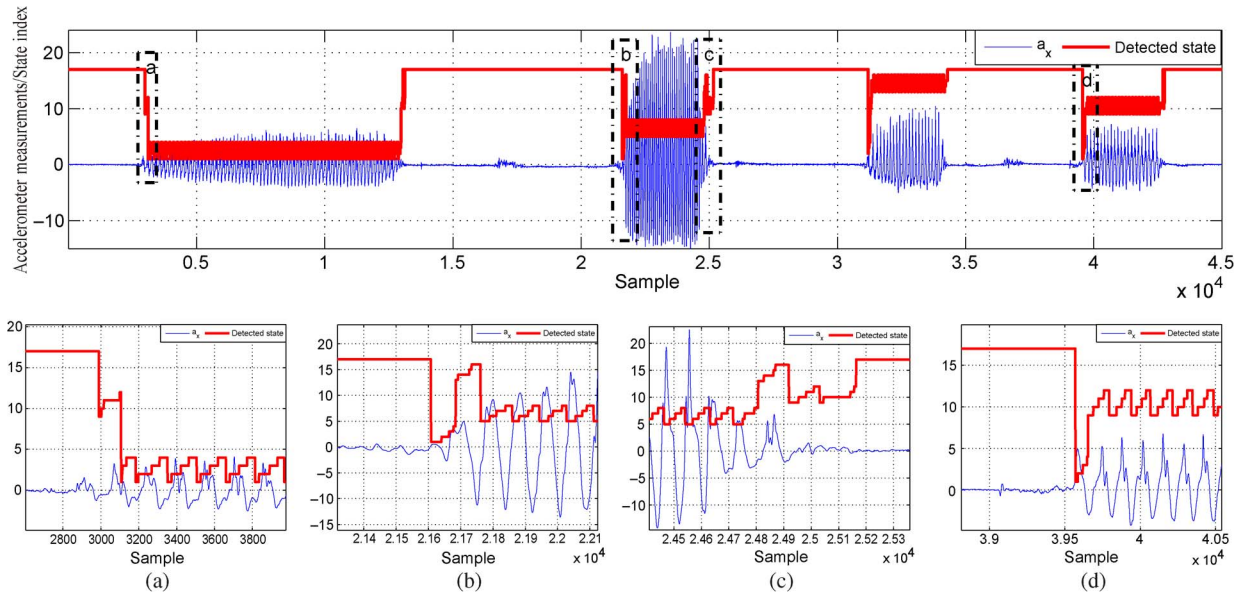

Fig. 11. First IMU output signal (a_x) for all the five defined motion states together with the classified gait phase based on the second method; see Section III-B1 (see Table III for the state indices). The corresponding IMU measurements are plotted in Fig. 9. Subfigures (a)–(d) illustrate the magnified demonstration of the specified parts of the signal with the corresponding box name.

TABLE IV
CONFUSION MATRIX OF ACTIVITY CLASSIFICATION USING THE FIRST PROPOSED METHOD. SEE SECTION III-B1

		Classified activity				
		Walking	Running	Going upstairs	Going downstairs	Standing
Actual activity	Walking	90%	0%	5%	5%	0%
	Running	0%	96%	2.7%	1.3%	0%
	Going upstairs	6%	0%	91%	3%	0%
	Going downstairs	6%	0%	4%	90%	0%
	Standing	0%	0%	1%	1%	98%

TABLE V
CONFUSION MATRIX OF ACTIVITY CLASSIFICATION USING THE SECOND PROPOSED METHOD. SEE SECTION III-B2

		Classified activity				
		Walking	Running	Going upstairs	Going downstairs	Standing
Actual activity	Walking	97.5%	0%	2%	0.5%	0%
	Running	0.5%	98.5%	1%	0%	0%
	Going upstairs	2.5%	0%	90%	7.5%	0%
	Going downstairs	1%	1%	2%	96%	0%
	Standing	0.5%	0%	0.3%	0.2%	99%

V. DISCUSSION

The main idea of this study was to devise an IMU setup that could potentially be used in vision-aided navigation systems and to present a method for both the activity classification and the joint activity and gait-phase classification. We proposed chest mounting the IMU and showed how the IMU signals for the Chem-IMU reveal cyclical patterns as does that for the lower body positioned IMU (see Fig. 3). Then, two HMM-based classifiers were introduced for the two aforementioned problems. Since no alternative solution is presented for this problem in the literature, the performances of the proposed algorithms were self-analyzed and compared both qualitatively and quantitatively. The conducted experiments with both of the classifiers showed a high probability of correct activity classification (around 95%). Thus, in addition to being a more suitable choice for the vision-aided navigation systems [1], [21], [45], Chem-IMU can be reliably used for both activity classification and gait analysis.

Although the two proposed methods are different in the feature extraction and exploited HMM structure, similar levels of accuracies were found for both of the provided methods with a marginally better correct performance obtained using the joint activity and gait-phase classification (see Tables IV and V). However, the main advantage of the latter scheme is the provision of gait analysis. For example, one interesting application of this probabilistic method is in step detection. In addition to the classic step detection approaches that cannot cover different walking patterns or irregular motions [26], [46], probabilistic methods can provide higher detection accuracy [24], [25]. Moreover, the delay in the output of the classification and the computational complexity are lower for the second proposed method. This is a consequence of the chosen time-frame length for DFT analysis in the first method.

Considering the performance of state-of-the-art activity classification methods (a correct classification rate between 85% and 99% [24], [30], [36], [40]), the achieved results imply that the Chem-IMU can be used for human activity classification with state-of-the-art performance. However, these methods are mainly developed for foot-mounted IMU, and if desired, in applying those to the Chem-IMU, special considerations might be required. Nevertheless, a comprehensive study comparing the Chem-IMU (upper body positioned IMU) and foot-mounted IMU (lower body positioned IMU), similar to [40], would be very informative and interesting but beyond the scope of this paper.

In our paper, we developed probabilistic activity classification methods that can be trained by a set of supervised subjects and activity scenarios. In contrast to the threshold-based [30], [31] and fuzzy logic methods [8], our HMM-based solutions can be easily applied to classify the measurements from new subjects with no further supervision.

There are a number of limitations to this study. First, subjects were asked to physically carry the acquisition device (a laptop connected to the IMU) with them; this might have forced them to change their normal movement slightly. Nevertheless, due to the probabilistic model of the measurements, it is expected that the performance in a normal life scenario remains close to the reported results. One additional weakness of the joint activity classification and gait analysis could be that the feature extraction is done in an *ad hoc* manner. A further study with more focus on feature extraction for this approach is therefore suggested.

VI. Conclusion

Low-complexity and accurate human activity monitoring is an important task both in navigation and biomedical applications. In this paper, a setup has been proposed for pedestrian activity classification and gait analysis using the measurements from a Chem-IMU. As the classification method, the continuous HMM with GMM output density functions has been used to classify the pedestrian activities. The additional gait-phase analysis is useful in health care and clinical applications to study the duration of each gait cycle and the step pattern of individuals. Moreover, the provided step information and the step number, together with the classified activity type, can be used to estimate the travel distance and dead reckoning for navigational purposes. The performance of the proposed methods has been evaluated by experimental data using the trained HMMs. The probability of the correct classification rate, based on our experiments, was about 0.95, with marginally better performance for the joint activity and gait classification method. This performance rate is comparable with the current state of the art and is good enough for different applications, e.g., as an interesting future investigative direction for visual–inertial navigation systems.

Acknowledgment

The authors would like to thank all the participants in the Signal Processing Lab and Communication Theory Lab at KTH, who kindly helped us in data collection.

References

[1] R. Jirawimut, S. Prakoonwit, F. Cecelja, and W. Balachandran, "Visual odometer for pedestrian navigation," *IEEE Trans. Instrum. Meas.*, vol. 52, no. 4, pp. 1166–1173, Aug. 2003.

[2] C.-W. Tan and S. Park, "Design of accelerometer-based inertial navigation systems," *IEEE Trans. Instrum. Meas.*, vol. 54, no. 6, pp. 2520–2530, Dec. 2005.

[3] M. Adams, W. Wijesoma, and A. Shacklock, "Autonomous navigation: Achievements in complex environments," *IEEE Instrum. Meas. Mag.*, vol. 10, no. 3, pp. 15–21, Jun. 2007.

[4] P. Händel, "Discounted least-squares gearshift detection using accelerometer data," *IEEE Trans. Instrum. Meas.*, vol. 58, no. 12, pp. 3953–3958, Dec. 2009.

[5] P. Händel, B. Enstedt, and M. Ohlsson, "Combating the effect of chassis squat in vehicle performance calculations by accelerometer measurements," *Measurement*, vol. 43, no. 4, pp. 483–488, May 2010.

[6] P. Szemes, H. Hashimoto, and P. Korondi, "Pedestrian-behavior-based mobile agent control in intelligent space," *IEEE Trans. Instrum. Meas.*, vol. 54, no. 6, pp. 2250–2257, Dec. 2005.

[7] A. Sabatini, C. Martelloni, S. Scapellato, and F. Cavallo, "Assessment of walking features from foot inertial sensing," *IEEE Trans. Biomed. Eng.*, vol. 52, no. 3, pp. 486–494, Mar. 2005.

[8] C. Senanayake and S. Senanayake, "Computational intelligent gait-phase detection system to identify pathological gait," *IEEE Trans. Inf. Technol. Biomed.*, vol. 14, no. 5, pp. 1173–1179, Sep. 2010.

[9] K. Aminian and B. Najafi, "Capturing human motion using body-fixed sensors: Outdoor measurement and clinical applications," *Comput. Animat. Virtual Worlds*, vol. 15, no. 2, pp. 79–94, May 2004.

[10] W. Wan, H. Liu, L. Wang, G. Shi, and W. Li, "A hybrid HMM/SVM classifier for motion recognition using μIMU data," in *Proc. IEEE Int. Conf. Robot. Biomimet.*, Dec. 2007, pp. 115–120.

[11] C. C. Yang and Y. L. Hsu, "A review of accelerometry-based wearable motion detectors for physical activity monitoring," *Sensors*, vol. 10, no. 8, pp. 7772–7788, 2010.

[12] A. Akl, C. Feng, and S. Valaee, "A novel accelerometer-based gesture recognition system," *IEEE Trans. Signal Process.*, vol. 59, no. 12, pp. 6197–6205, Dec. 2011.

[13] H. Vathsangam, A. Emken, E. Schroeder, D. Spruijt-Metz, and G. Sukhatme, "Determining energy expenditure from treadmill walking using hip-worn inertial sensors: An experimental study," *IEEE Trans. Biomed. Eng.*, vol. 58, no. 10, pp. 2804–2815, Oct. 2011.

[14] Ö. Bebek, M. A. Suster, S. Rajgopal, M. J. Fu, X. Huang, M. C. Cavusoglu, D. J. Young, M. Mehregany, A. J. Van Den Bogert, and C. H. Mastrangelo, "Personal navigation via high-resolution gait-corrected inertial measurement units," *IEEE Trans. Instrum. Meas.*, vol. 59, no. 11, pp. 3018–3027, Nov. 2010.

[15] G. Panahandeh, I. Skog, and M. Jansson, "Calibration of the accelerometer triad of an inertial measurement unit, maximum likelihood estimation and Cramer-Rao bound," in *Proc. IEEE Int. Conf. IPIN*, Sep. 2010, pp. 1–6.

[16] A. Jimenez Ruiz, F. Seco Granja, J. Prieto Honorato, and J. Guevara Rosas, "Accurate pedestrian indoor navigation by tightly coupling foot-mounted IMU and RFID measurements," *IEEE Trans. Instrum. Meas.*, vol. 61, no. 1, pp. 178–189, Jan. 2012.

[17] I. Skog and P. Händel, "In-car positioning and navigation technologies—A survey," *IEEE Trans. Intell. Transp. Syst.*, vol. 10, no. 1, pp. 4–21, Mar. 2009.

[18] J. Fang and X. Gong, "Predictive iterated Kalman filter for INS/GPS integration and its application to SAR motion compensation," *IEEE Trans. Instrum. Meas.*, vol. 59, no. 4, pp. 909–915, Apr. 2010.

[19] D. Grejner-Brzezinska, C. Toth, H. Sun, X. Wang, and C. Rizos, "A robust solution to high-accuracy geolocation: Quadruple integration of GPS, IMU, pseudolite, and terrestrial laser scanning," *IEEE Trans. Instrum. Meas.*, vol. 60, no. 11, pp. 3694–3708, Nov. 2011.

[20] N. El-Sheimy, K.-W. Chiang, and A. Noureldin, "The utilization of artificial neural networks for multisensor system integration in navigation and positioning instruments," *IEEE Trans. Instrum. Meas.*, vol. 55, no. 5, pp. 1606–1615, Oct. 2006.

[21] G. Panahandeh, D. Zachariah, and M. Jansson, "Exploiting ground plane constraints for visual-inertial navigation," in *Proc. IEEE-ION PLANS*, 2012, pp. 527–534.

[22] E. Foxlin, "Pedestrian tracking with shoe-mounted inertial sensors," *IEEE Comput. Graph. Appl.*, vol. 25, no. 6, pp. 38–46, Nov./Dec. 2005.

[23] J. Rantakokko, J. Rydell, P. Stromback, P. Händel, J. Callmer, D. Tornqvist, F. Gustafsson, M. Jobs, and M. Gruden, "Accurate and reliable soldier and first responder indoor positioning: Multisensor systems and cooperative localization," *IEEE Wireless Commun.*, vol. 18, no. 2, pp. 10–18, Apr. 2011.

[24] Z. Sun, X. Mao, W. Tian, and X. Zhang, "Activity classification and dead reckoning for pedestrian navigation with wearable sensors," *Meas. Sci. Technol.*, vol. 20, no. 1, pp. 015203-1–015203-10, Jan. 2009.
[25] X. Chen, S. Hu, Z. Shao, and J. Tan, "Pedestrian positioning with physical activity classification for indoors," in *Proc. IEEE ICRA*, May 2011, pp. 1311–1316.
[26] L. Fang, P. Antsaklis, L. Montestruque, M. McMickell, M. Lemmon, Y. Sun, H. Fang, I. Koutroulis, M. Haenggi, M. Xie, and X. Xie, "Design of a wireless assisted pedestrian dead reckoning system—The NavMote experience," *IEEE Trans. Instrum. Meas.*, vol. 54, no. 6, pp. 2342–2358, Dec. 2005.
[27] A. Bourke, J. O'Brien, and G. Lyons, "Evaluation of a threshold-based tri-axial accelerometer fall detection algorithm," *Gait Posture*, vol. 26, no. 2, pp. 194–199, Jul. 2007.
[28] J. Chen, K. Kwong, D. Chang, J. Luk, and R. Bajcsy, "Wearable sensors for reliable fall detection," in *Proc. IEEE-EMBS 27th Annu. Int. Conf. Eng. Med. Biol. Soc.*, Jan. 2005, pp. 3551–3554.
[29] W. Zijlstra and A. L. Hof, "Assessment of spatio-temporal gait parameters from trunk accelerations during human walking," *Gait Posture*, vol. 18, no. 2, pp. 1–10, Oct. 2003.
[30] I. P. I. Pappas, M. R. Popovic, T. Keller, V. Dietz, and M. Morari, "A reliable gait phase detection system," *IEEE Trans. Neural Syst. Rehabil. Eng.*, vol. 9, no. 2, pp. 113–125, Jun. 2001.
[31] B. Smith, D. Coiro, R. Finson, R. Betz, and J. McCarthy, "Evaluation of force-sensing resistors for gait event detection to trigger electrical stimulation to improve walking in the child with cerebral palsy," *IEEE Trans. Neural Syst. Rehabil. Eng.*, vol. 10, no. 1, pp. 22–29, Mar. 2002.
[32] Z. Liu and C.-H. Won, "Knee and waist attached gyroscopes for personal navigation: Comparison of knee, waist and foot attached inertial sensors," in *Proc. IEEE/ION PLANS*, May 2010, pp. 375–381.
[33] G. Panahandeh and M. Jansson, "Vision-aided inertial navigation using planar terrain features," in *Proc. IEEE Int. Conf. Robot, Vis. Signal Process.*, Sep. 2011, pp. 287–291.
[34] C. Hide, T. Botterill, and M. Andreotti, "Low cost vision-aided IMU for pedestrian navigation," in *Proc. UPINLBS*, Oct. 2010, pp. 1–7.
[35] S. K. Park and Y. S. Suh, "A zero velocity detection algorithm using inertial sensors for pedestrian navigation systems," *Sensors*, vol. 10, no. 10, pp. 9163–9178, 2010.
[36] G. Shi, Y. Zou, Y. Jin, X. Cui, and W. Li, "Towards HMM based human motion recognition using MEMS inertial sensors," in *Proc. IEEE Int. Conf. ROBIO*, Feb. 2009, pp. 1762–1766.
[37] G. Panahandeh, N. Mohammadiha, A. Leijon, and P. Händel, "Chest-mounted inertial measurement unit for pedestrian motion classification using continuous hidden Markov model," in *Proc. IEEE I2MTC*, May 2012, pp. 991–995.
[38] M. Chen, B. Huang, and Y. Xu, "Human abnormal gait modeling via hidden Markov model," in *Proc. IEEE ICIA*, Jul. 2007, pp. 517–522.
[39] M. Susi, D. Borio, and G. Lachapelle, "Accelerometer signal features and classification algorithms for positioning applications," in *Proc. Int. Tech. Meeting Inst. Navig.*, San Diego, CA, Jan. 2011, pp. 158–169.
[40] S. Preece, J. Goulermas, L. Kenney, and D. Howard, "A comparison of feature extraction methods for the classification of dynamic activities from accelerometer data," *IEEE Trans. Biomed. Eng.*, vol. 56, no. 3, pp. 871–879, Mar. 2009.
[41] M. Asgharioskoei and H. Hu, "Myoelectric control systems—A survey," *Biomed. Signal Process. Control*, vol. 2, no. 4, pp. 275–294, Oct. 2007.
[42] J. Bilmes, "A gentle tutorial of the EM algorithm and its application to parameter estimation for Gaussian mixture and hidden Markov models," Univ. California, Berkeley, CA, TR-97-021 Rep., 1997, tech. rep..
[43] A. P. Dempster, N. Laird, and D. B. Rubin, "Maximum likelihood from incomplete data via the EM algorithm," *J. R. Stat. Soc.*, vol. 39, no. 1, pp. 1–38, 1977.
[44] L. Rabiner, "A tutorial on hidden Markov models and selected applications in speech recognition," *Proc. IEEE*, vol. 77, no. 2, pp. 257–286, Feb. 1989.
[45] N. Kyriakoulis and A. Gasteratos, "Color-based monocular visuoinertial 3-d pose estimation of a volant robot," *IEEE Trans. Instrum. Meas.*, vol. 59, no. 10, pp. 2706–2715, Oct. 2010.
[46] S. Godha, G. Lachapelle, and M. Cannon, "Integrated GPS/INS system for pedestrian navigation in a signal degraded environment," in *Proc. 19th ION GNSS*, Sep. 2006, pp. 2151–2164.

Ghazaleh Panahandeh (S'11) received the M.S. degree in electronics engineering from the Sharif University of Technology, Tehran, Iran, in 2008. She is currently working toward the Ph.D. degree in telecommunications in the Signal Processing Laboratory, KTH Royal Institute of Technology, Stockholm, Sweden.

Her research interests include inertial navigation and positioning, vision-aided inertial navigation, estimation theory, and stochastic signal processing.

Nasser Mohammadiha (S'11) received the M.Sc. degree in electronics engineering from the Sharif University of Technology, Tehran, Iran, in 2006. He is currently working toward the Ph.D. degree in the telecommunications in the Sound and Image Processing Laboratory, KTH Royal Institute of Technology, Stockholm, Sweden.

He worked on digital hardware and software design until 2008. His research interests include speech processing, mainly speech enhancement, image processing, and statistical signal modeling.

Arne Leijon (M'10) received the M.S. degree in engineering physics and the Ph.D. degree in information theory from the Chalmers University of Technology, Gothenburg, Sweden, in 1971 and 1989, respectively.

He has been a Professor of hearing technology with the Sound and Image Processing Laboratory, KTH Royal Institute of Technology, Stockholm, Sweden, since 1994. His main research interest concerns applied signal processing in aids for people with hearing impairment, and methods for individual fitting of these aids, based on psychoacoustic modeling of sensory information transmission and subjective sound quality.

Peter Händel (S'88–M'94–SM'98) received the Ph.D. degree from Uppsala University, Uppsala, Sweden, in 1993.

From 1987 to 1993, he was with Uppsala University. From 1993 to 1997, he was with Ericsson AB, Kista, Sweden. From 1996 to 1997, he was also with the Tampere University of Technology, Tampere, Finland. Since 1997, he has been with the Royal Institute of Technology, Stockholm, Sweden, where he is currently a Professor of Signal Processing. From 2000 to 2006, he worked part time with the Swedish Defence Research Agency. In 2010, he spent some time at the Indian Institute of Science, Bangalore, India, as a Guest Professor. He is currently a Guest Professor with the University of Gävle, Gävle, Sweden.

Dr. Händel has served as an Associate Editor for the IEEE TRANSACTIONS ON SIGNAL PROCESSING.